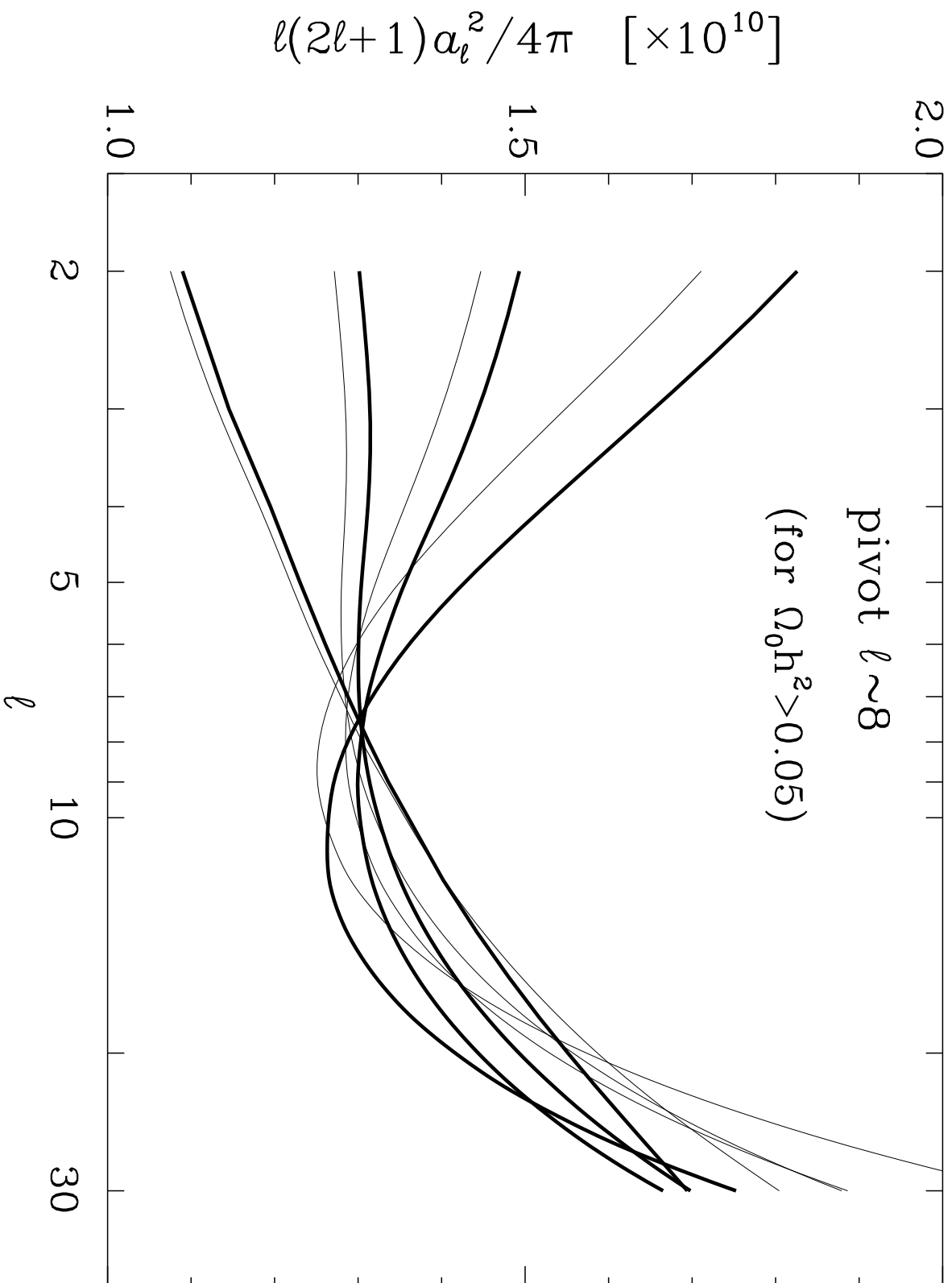


This figure "fig1-1.png" is available in "png" format from:

<http://arxiv.org/ps/astro-ph/9502035v1>

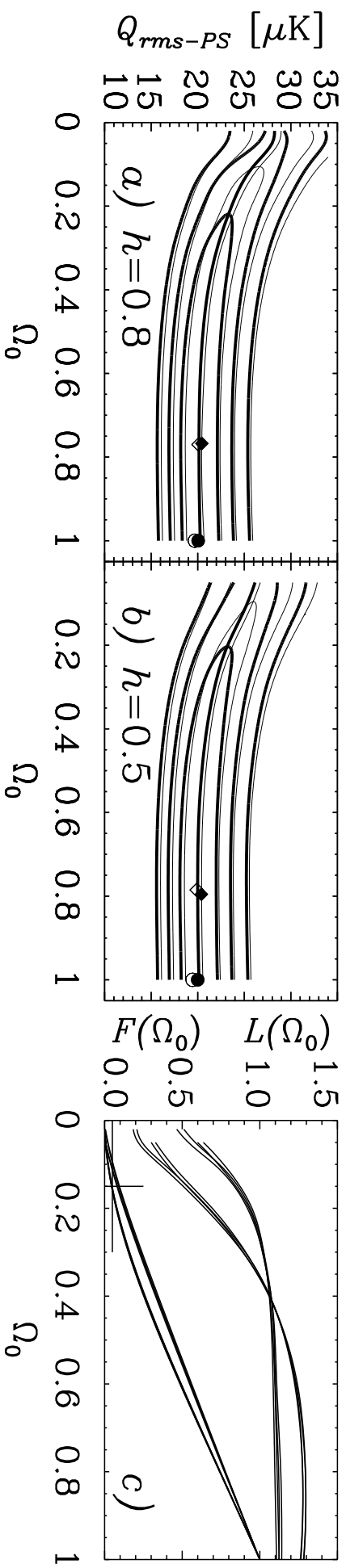
This figure "fig2-1.png" is available in "png" format from:

<http://arxiv.org/ps/astro-ph/9502035v1>



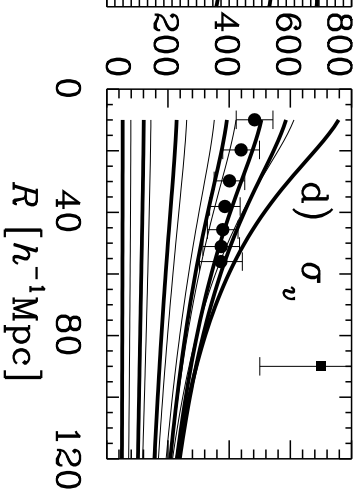
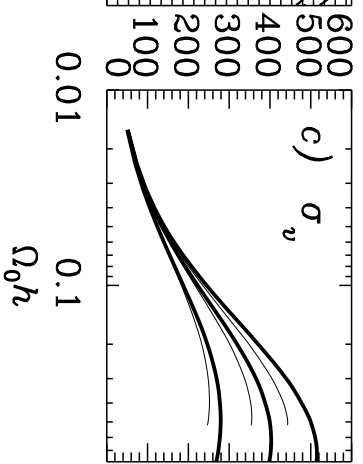
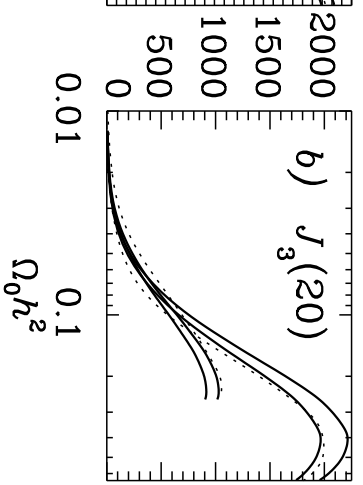
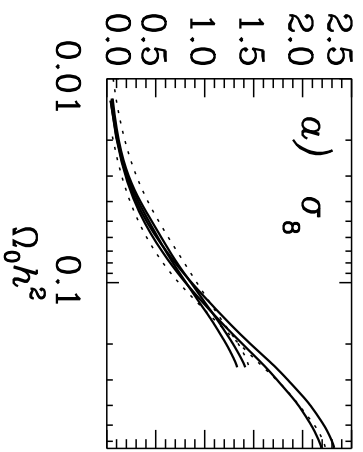
This figure "fig1-2.png" is available in "png" format from:

<http://arxiv.org/ps/astro-ph/9502035v1>



This figure "fig1-3.png" is available in "png" format from:

<http://arxiv.org/ps/astro-ph/9502035v1>



This figure "fig1-4.png" is available in "png" format from:

<http://arxiv.org/ps/astro-ph/9502035v1>

# COBE-DMR-NORMALISATION FOR COSMOLOGICAL CONSTANT DOMINATED COLD DARK MATTER MODELS

Radosław Stompor<sup>1,5</sup>, Krzysztof M. Górski<sup>2,3</sup>, and Anthony J. Banday<sup>4</sup>

## ABSTRACT

The two-year *COBE*-DMR 53 and 90 GHz sky maps are used to determine the normalization of inflationary, cosmological constant dominated, cold dark matter models. Although the *COBE*-DMR data prefer a nearly critical value for the total density, low-density models with  $\Omega_0 \geq 0.15$  can not be rejected at a confidence level  $\gtrsim 95\%$ . We compare theoretical predictions for various large scale statistics, computed for a range of values of  $\Omega_0$  and  $h = 0.5$ , or  $0.8$ , to various measures of structure in the universe.

*Subject headings:* cosmic microwave background — cosmology: observations — large-scale structure of the universe

Submitted to *Astrophysical Journal Letters*

---

<sup>1</sup> Copernicus Astronomical Center, Bartycka 18, 00-716 Warszawa, Poland

<sup>2</sup> Universities Space Research Association, NASA/GSFC, Laboratory for Astronomy and Solar Physics, Code 685, Greenbelt, MD 20771

<sup>3</sup> Warsaw University Observatory, Aleje Ujazdowskie 4, 00-478 Warszawa, Poland

<sup>4</sup> Hughes STX Corporation, 4400 Forbes Bldg, Lanham, MD 20706

<sup>5</sup> email: radek@camk.edu.pl

## 1. Introduction

Cosmological constant dominated, spatially flat, cold dark matter models (CDM- $\Lambda$ ) can be considered a natural extension of the standard cold dark matter (CDM) scenario. By adjusting the combination of a non-zero cosmological constant and the total matter density parameter,  $\Omega_0$  (which remains poorly constrained by observations), we can maintain the spatial flatness of the universe required by the inflationary paradigm, whilst striving to improve the agreement of the theoretical model predictions to the observational data (Peebles 1984; Efstathiou, Maddox, & Sutherland 1990; Carrol, Press, & Turner 1992; Kofman, Gnedin, & Bahcall 1993).

In this *Letter*, we normalise the CDM- $\Lambda$  models to the two year *COBE*-DMR anisotropy measurements (Bennett et al. 1994), using the linear angular power spectrum estimation technique of Górski (1994)<sup>†</sup>. Subsequently, we discuss the predictions of these appropriately normalised models for various large-scale structure measures.

## 2. CMB Anisotropy Normalisation Procedure

The data selection and power spectrum inference technique were implemented exactly as described in Górski et al. (1994), and Górski, Stompor, & Banday (1995).

### 2.1 Theoretical Spectra of Anisotropy

We consider spatially flat models with non-zero cosmological constant ( $\Omega_0 + \lambda = 1$ ) and primordial perturbations as prescribed (to within an arbitrary amplitude) by the inflationary scenario. Hence, random-phase, Gaussian, scalar curvature perturbations are assumed (no gravity waves), corresponding to adiabatic density perturbations with the Harrison-Zel'dovich power spectrum,  $P(k) \propto k$ . The cosmological models considered are specified as follows: 1) The value of the Hubble constant,  $H_0 = 100\text{km s}^{-1} \text{Mpc}^{-1}$ , is taken to be given by either  $h = 0.5$  or  $0.8$ . 2) In agreement with Big Bang nucleosynthesis (BBN) constraints —  $\Omega_b h^2 = 0.013$  (Reeves 1994) — we consider a baryon density  $\Omega_b = 0.05$  for  $h=0.5$ , or  $\Omega_b = 0.02$  for  $h = 0.8$ . For comparison we also consider models with  $\Omega_b = 0.03$  for both values of  $h$ . 3) The total density,  $\Omega_0$ , is varied between  $\Omega_b$  and unity and the value of  $\lambda$  adjusted to retain a flat global geometry.

The CMB anisotropy multipole coefficients and the matter perturbation transfer functions were computed using numerical Boltzman code as described in Stompor (1994) by

---

<sup>†</sup> See also Bunn & Sugiyama (1994).

integrating the evolution equations until a redshift  $z = 0$ . Thus all effects caused by the cosmological constant were taken into account exactly.

Figure 1 shows several of the CDM- $\Lambda$  radiation power spectra normalised to the two year *COBE*-DMR anisotropy. At low- $\ell$  ( $\lesssim 10$ ), the radiation power spectra are determined by both the usual Sachs & Wolfe (1967, SW) and the cosmological constant induced, integrated SW (ISW) effects (Kofman & Starobinskii 1985, Górski, Silk, & Vittorio 1992), and depend very weakly on the Hubble constant. Over the range  $10 \lesssim \ell \lesssim 30$ , an additional ISW effect, due to the non-negligible radiation energy density contribution to the total density after decoupling, is a significant factor in determining the shape of the anisotropy spectrum and introduces a noticeable dependence on  $h$ . The strength of both ISW effects falls with increasing  $\Omega_0$  †. Consequently the power spectra flatten as  $\Omega_0$  increases, and for models with near critical matter density the spectra monotonically grow with  $\ell$ .

We express the power spectrum amplitude in terms of  $Q_{rms-PS}$ , the value of the exactly computed quadrupole,  $a_2$ , multiplied by  $(5/4\pi)^{1/2}$ , which depends non-trivially on cosmological parameters. This is a generalisation of the normalisation introduced in Smoot *et al.* (1992) for pure power law model spectra. For  $\Omega_0 \lesssim 0.5$ , the ISW contributions boost the quadrupole over its pure SW value. For  $\Omega_0 \gtrsim 0.5$  — models with a negligible cosmological constant induced ISW effect — the resulting exact quadrupole is lower than its pure SW counterpart (see Table 1). The steepest spectra arise in models near critical matter density ( $\Omega_0 \simeq 0.8$ ).

### 2.3 Results of $Q_{rms-PS}$ Fitting

Likelihood contours in the  $Q_{rms-PS} - \Omega_0$  plane (under the assumption of a uniform prior) are shown in Figs. 2*a*, *b*. The preferred value of the matter density is clearly close to critical, but even low-density models with  $\Omega_0 \sim 0.1$  lie well within the 95% confidence limits and appear acceptable.

A typical likelihood fit for fixed  $\Omega_0$  yields a  $\sim 13\sigma$  determination of  $Q_{rms-PS}$  ( $\sim 20 - 26\mu\text{K}$ ). Systematic effects, as discussed in Górski, Stompor, & Banday (1995) and

---

† However, in critical density models, only the cosmological constant induced ISW disappears. Furthermore, the ISW effect due to the radiation density contribution though usually small, is not negligible, and results in the steepening of the low- $\ell$  end of the power spectrum (Bond 1993; Bunn, Scott, & White 1994; Górski, Stompor, & Banday 1995).

associated with 1) different coordinate frames (galactic/ecliptic) used for the *COBE*-DMR data representation and 2) inclusion/exclusion of the quadrupole, are observed to shift the value of the best-fit normalisation by  $\sim 0.8 \mu\text{K}$  and  $0.4 \mu\text{K}$ , respectively. Nevertheless, they do not influence any conclusions regarding the acceptability of the low- $\Omega_0$  models, and the lower limit of  $\Omega_0 \geq 0.15$  is the most restrictive one. (Interestingly, this limit does not depend on  $h$  though the *COBE*-DMR normalised  $Q_{rms-PS}$  does.)

A convenient summary of the inferred normalisation encompassing statistical errors, systematic shifts, and cosmological parameter dependences is then,  $Q_{rms-PS} \simeq \{[20 + 9.1h^{0.6} \exp(-\Omega_0^2 h^{0.3}/0.057)] \times (1 \pm 0.077) \pm 0.4 \pm 0.2 \pm 0.25\} \mu\text{K}$ . Exact values for a representative set of CDM- $\Lambda$  models can be found in Table 1, which can be easily interpolated to other models with high accuracy. However, our fit is good to within 5%.

Note that, unlike in power-law or critical density models (Górski *et al.* 1994; Górski Stompor, & Banday 1995), there is no pivot point at a particular multipole order common to all of the models considered. Nevertheless, for those models with  $\Omega_0 h^2 \gtrsim 0.05$ , a good approximate pivot can be found at  $l \simeq 8$  (Fig. 1), yielding the convenient model-independent normalisation  $a_8 \simeq 9.5 \pm 0.73 \mu\text{K}$ .

Since the dependence of the fitted  $Q_{rms-PS}$  amplitude on model parameters is rather weak, and because the SW and ISW effects scale with the total density, there is a strong resulting variation with  $\Omega_0$  of the amplitudes of the matter power spectra, as shown in Fig. 4.

### 3. Measures of Large-Scale Structure

Having determined the *COBE*-DMR normalisations for our grid of CDM- $\Lambda$  models, we now discuss the values of several large-scale structure statistics computed from the matter perturbation spectra. Hereafter, we apply the usual definitions:  $(\sigma_{hR})_{mass}^2 = (1/2\pi^2) \int_0^\infty dk k^2 W_{TH}^2(kR) P(k)$ , and  $J_3(hR) = (R^3/2\pi^2) \int_0^\infty dk k^2 W_{TH}(kR) P(k)$ , where  $P(k)$  is the matter power spectrum and  $W_{TH}(x) = 3j_1(x)/x$ . Representative values of large scale structure measures derived from the models are included in Table 1.

#### 3.1 Mass Fluctuations: $\sigma_8$ and $J_3$

The high values of  $(\sigma_8)_{mass} > 1$  predicted from the *COBE*-DMR normalised  $\Omega_0 = 1$ , CDM models (Bunn, Scott, & White 1994, Górski, Stompor, & Banday 1995) are difficult to reconcile with observations of the fluctuations in the number density of galaxies,  $(\sigma_8)_{gal} \simeq 0.8 - 1$  (e.g. Davis & Peebles 1983; Fisher et al. 1993; Feldman, Kaiser & Peacock

1994; and Baugh & Efstathiou, 1993). At face value, this would require that the biasing parameter,  $b = (\sigma_8)_{gal}/(\sigma_8)_{mass}$ , be somewhat smaller than unity, in direct disagreement with the estimates inferred from galaxy cluster catalogs (Henry & Arnaud 1991; White, Efstathiou, & Frenk 1993) and from the galaxy pair-wise velocities (Davis *et al.* 1985, Cen & Ostriker 1992). A non-vanishing cosmological constant provides a means to circumvent these problems. The predicted  $(\sigma_8)_{mass}$  as a function of  $\Omega_0 h^2$  is shown in Fig. 3*a*. A low value of  $\Omega_0$  suppresses peculiar motions so high bias is not required to fit the small-scale galaxy pair-wise velocities. Thus unbiased models with  $(\sigma_8)_{mass} \simeq (\sigma_8)_{gal}$  are likely to be of interest. However, physical motivations for requiring a biasing parameter somewhat larger than unity were discussed early on (e.g. Silk 1977), and are supported by recent hydrodynamical simulations (Katz, Hernquist & Weinberg 1992, Cen & Ostriker 1992) suggesting a value  $b \sim 1.5$ . In what follows, we conservatively discuss all values of  $b \geq 1$ . Models with  $\Omega_0 h^2 \lesssim 0.12$  then seem to be particularly interesting.

Comparison of the  $J_3$ -integral, computed on the larger scale of  $R = 20h^{-1}\text{Mpc}$  (and, therefore, more adequately modelled than  $(\sigma_8)_{mass}$  by our linear approach), to the observational value from Davis & Peebles (1983),  $J_3(20h^{-1}\text{Mpc}) \simeq 700 h^{-3} \text{Mpc}^3$  (probably accurate to within  $\sim 30\%$ ), also seems to favour the low- $\Omega_0$  CDM- $\Lambda$  -models (Fig. 3*b*) in agreement with above constraint.

### 3.2 Large-Scale Flows

The rms amplitudes of large-scale bulk flows (Fig. 3*c, d*) are modelled as  $\sigma_v^2(R) = (2\pi^2)^{-1} H_0^2 f(\Omega_0) \int dk P(k) W_{BF}^2(k, R)$ , where  $W_{BF} = W_{TH}^2(kR) \exp(-k^2 r_s^2)$  is a model independent, POTENT-like window function as shown in Fig. 4 ( $r_s = 12h^{-1}\text{Mpc}$ ). The factor  $f(\Omega_0) \approx \Omega^{0.6} + (1 + \Omega_0/2)\lambda/70$  as computed by Lahav *et al.* (1991) approximately describes the suppression of the velocity field in low- $\Omega_0$  CDM- $\Lambda$  models<sup>†</sup>. In Fig. 3*d*, the POTENT (Dekel 1994) and Lauer & Postman (1994) data are also shown. It is apparent that all models with  $\Omega_0 h \gtrsim 0.1$  can account for the POTENT velocities. However, if the Lauer & Postman data are confirmed even the critical density models will be in serious trouble.

---

<sup>†</sup> In our calculations we smooth the velocity field obtained from the numerical integration of the propagation equations, and these are the values given in Table 1. The Lahav *et al.* approximation is used for illustrative purposes, although it works well for  $\Omega_0 \gtrsim 0.1$ .

### 3.3 Galaxy and Matter Distribution Power Spectra

Comparison of the theoretical matter power spectra with those inferred from the empirical data should, in principle, be the most complete and informative method possible. However, such a procedure is hampered by a number of factors, including the linear nature of our theoretical computations and the lack of agreement between different observational estimates of the galaxy power spectrum (which may be explicable in terms of intrinsic variations in the survey samples and/or by differences in the estimation technique utilised). In spite of such difficulties, we still consider such a comparison, shown in Fig. 4, to be informative in a qualitative way.

On small scales ( $k > 0.1h^{-1}\text{Mpc}$ ), the estimated power spectra from Baugh & Efstathiou (1994), Peacock & Dodds (1994) and the IRAS 1.2 Jy redshift survey are in reasonable agreement for those models with  $\Omega_0 h^2 \lesssim 0.075$ . This limit is somewhat more restrictive than that obtained previously, and, combined with the *COBE*-DMR plus *POTENT* inferred lower limits on  $\Omega_0$ , leaves little room for a successful model. However, the results of da Costa *et al.* (1994) show enhanced power on scales  $k \gtrsim 0.1h^{-1}\text{Mpc}^{-1}$ , contrary to the expectation that such redshift space derived quantities underestimate the real space power spectra (Gramann *et al.* 1993). The observed discrepancies, particularly with respect to the similarly redshift-space-derived IRAS values, can not be solely ascribed to redshift space induced distortions. The relaxation of the above constraint would therefore seem to be in order until the observational situation is clarified. Conservatively, we retain the previously established relations.

However, it then appears that the preferred models can not simultaneously fit the large-scale behaviour indicated by the APM data. This is more properly described by an unbiased CDM  $h = 0.5$  model, which, unfortunately, fails noticeably on smaller scales. One should note, however, that on these larger scales there is again pronounced disagreement between different data sets (with the SSRS2+CfA2 data of da Costa *et al.*, 1994, clearly overshooting all other estimates by a factor  $\sim$  four, which cannot be completely explained by the effect of projecting the power spectrum to redshift space<sup>†</sup>). It undoubtedly remains

---

<sup>†</sup> This would require  $b \lesssim 2\Omega_0^{0.56}/5 < 1$ . For values of  $b$  in the range  $\simeq 1 - 2$ , the linear correction appropriate for scales  $k \lesssim 0.03h\text{Mpc}^{-1}$  (Gramann, Cen & Bahcall 1993) is only 10%-30% for  $\Omega_0 = 0.1$  and 20%-50% for  $\Omega_0 = 0.4$  so the pronounced power enhancement survives.

too early for any definitive conclusions to be reached. If the SSRS2+CfA2 data are confirmed, the power enhancement visible on scales  $k \sim 0.01 h\text{Mpc}^{-1}$  may favour the low- $\Omega_0$  CDM- $\Lambda$  models. Improved, very deep galaxy catalogs may provide us with a definitive test of CDM- $\Lambda$  models.

#### 4. Discussion

In this *Letter*, we reconsider the CDM- $\Lambda$  models normalised to the two year *COBE*-DMR anisotropy data. We show that the low- $\Omega_0$  CDM- $\Lambda$  (with  $\Omega_0 \geq 0.15$ ) models can not be rejected solely on the basis of the *COBE*-DMR data, although the most likely  $\Omega_0$  value is strikingly close to unity (see also Bunn & Sugiyama 1994). Conversely, observations of the matter distribution do require low values of the total density resulting in the constraint  $\Omega_0 h^2 \lesssim 0.12$ . On larger scales, these models predict bulk flows in reasonable agreement with POTENT for  $\Omega_0 h \gtrsim 0.1$ , but dramatically smaller than determined by the Lauer & Postman analysis for any ( $\leq 1$ ) value of  $\Omega_0$ . Therefore, if the latter observation is confirmed all CDM- $\Lambda$  models (together with critical density CDM or MDM models) will be found wanting. The predicted mass distribution on scales of a few hundred Mpc overshoots most of the experimental estimates (including those derived from the IRAS 1.2Jy & APM surveys), but is in rough agreement with that recently obtained by da Costa *et al.* (1994).

At present, although the position of the CDM- $\Lambda$  models is more comfortable than that of critical density models, it is not free from potentially fatal flaws. Unfortunately, CMB anisotropies on a one degree scale do not offer any serious prospects for distinguishing between cosmological constant models and other viable scenarios (Bond et al. 1994). Hence, definite conclusions will have to await more reliable observational data, particularly large-scale, deep galaxy surveys capable of unraveling the shape of the galaxy power spectrum on scales down to  $k \sim 0.01 h\text{Mpc}^{-1}$  (ie. comoving length-scales up to  $\sim 600 h^{-1}\text{Mpc}$ ).

We acknowledge the efforts of those contributing to the *COBE*-DMR. This work was supported in part by the Office of Space Sciences of NASA Headquarters. R. Stompor acknowledges LASP/COBE support during his stay at Goddard when this work was conducted. We are grateful to L. da Costa, K. Fisher and M. Vogeley for providing their power spectra, and A. Dekel for providing the bulk flow data.

## REFERENCES

- Baugh, C.M., & Efstathiou, G.P. 1993, MNRAS, 265, 145
- Bennett, C. L., et al. 1994, ApJ, 436, 423
- Bond, J. R. 1993, in Proc. of the IUCAA Dedication Ceremonies, ed. T. Padmanabhan, New York:John Wiley & Sons, in press
- Bond, J.R., Crittenden, R., Davies, R.L., Efstathiou, G., & Steinhardt, P.J. 1994, Phys.-Rev.Lett., 72, 13
- Bunn, E., & Sugiyama, N. 1994, Berkeley preprint CfPA-TH-94-33
- Bunn, E., Scott, D., & White, M. 1994, Berkeley preprint CfPA-94-TH-42, astro-ph-9409003
- Carrol, S.M., Press, W.H., & Turner, E.L. 1992 ARA&A, 30, 499
- Cen, R., & Ostriker, J. P. 1992, ApJ,399, L113
- Davis, M. & Peebles, P.J.E. 1983, ApJ, 267, 465
- Dekel, A. 1994, ARA&A, 32, 371
- da Costa, L.N., Vogley, M.S., Geller, M.J., Huchra, J.P., & Park, C.P. 1994, ApJ, 437, L1
- Efstathiou, G.P., Bond, J.R., & White, S.D.M. 1992, MNRAS, 258, 1P
- Efstathiou, G., Maddox, S.J., & Sutherland, W.J. 1990, Nature, 348, 705
- Feldman, H.A., Kaiser, N., & Peacock, J.A. 1994, ApJ, 426, 23
- Fisher, K.B., Davis, M., Strauss, M.A., Yahil, A., & Huchra, J.P. 1993, ApJ, 402, 42
- Górski, K. M. 1994, ApJ, 430, L85
- Górski, K. M., et al. 1994, ApJ, 430, L89
- Górski, K. M., Silk, J., & Vittorio, N. 1992, Phys.Rev.Lett., 68, 733
- Gramann, M., Cen, R., & Bahcall, N. A. 1993 ApJ, 419, 440
- Henry, J.P., & Arnaud, K.A. 1991, ApJ, 372, 410
- Katz, N., Hernquist, L., & Weinberg, D. H. 1992, ApJ, 399, L109
- Kofman, L.A., Gnedin, N.Y., & Bahcall, N.A. 1993, ApJ, 413, 1
- Kofman, L.A., & Starobinskii, A.A. 1985, Sov.Astron., 11, L5
- Lahav, O., Lilje, P. B., Primack, J. R., & Rees, M. J. 1991, MNRAS, 251, 128
- Lauer, T. R., & Postman, M. 1994, ApJ, 425, 418
- Peacock, J. A., & Dodds, S. J. 1994, MNRAS, 267, 1020
- Peebles, P.J.E. 1984, ApJ, 284, 439
- Reeves, H. 1994, Rev. Mod. Phys., 66, 193
- Sachs, R.K., & Wolfe, A.M. 1967, ApJ, 147, 73
- Silk, J. 1977, ApJ, 211, 638
- Smoot, G.F., et al. 1992, ApJ, 396, L1
- Stompor, R. 1994, A&A, 287(III), 693
- White, S. D. M., Efstathiou, G., & Frenk, C. S. 1993, MNRAS, 262, 1023

## FIGURE CAPTIONS

Fig. 1.— CDM- $\Lambda$  CMB anisotropy power spectra normalised to *COBE*-DMR. The thin lines correspond to the  $h = 0.5, \Omega_b = 0.05$  models, thick lines to models with  $h = 0.8, \Omega_b = 0.02$ . The curves are drawn for four values of total density (in descending order at  $\ell = 2$ ):  $\Omega_0 = 0.1, 0.2, 0.3, 1$ . The approximate pivot point (for  $\Omega_0 h^2 \gtrsim 0.05$  models) is also shown.

Fig. 2.— *a)* Contour plots of the likelihood density in the  $Q_{rms-PS} - \Omega_0$  plane for the  $h = 0.8$  CDM- $\Lambda$  models determined from analysis of the two year *COBE*-DMR data in ecliptic coordinates. 68%, 95%, and 99.8% integrated likelihood levels, derived under the assumption of a uniform  $(Q_{rms-PS}, \Omega_0)$ -prior, and the  $\Omega_0 = \text{const}$ -ridge lines are shown. Thick lines correspond to the results of the analysis with the quadrupole included, thin lines excluding the quadrupole. Diamonds show the loci of the likelihood maxima: filled symbols show the situation when the quadrupole is included, open symbols when it is excluded. The filled and open circles show the likelihood maxima loci derived from analysis of the galactic data to illustrate the small shift in the inferred model amplitude. *b)* As in *a* for  $h = 0.5$ . *c)* Marginal likelihood densities for  $\Omega_0$ , derived by integration of the two dimensional density distributions (from panels *a* and *b*) over  $Q_{rms-PS}$ , are shown by thin lines. The functions corresponding to the analysis with the quadrupole included fall more steeply with decreasing  $\Omega_0$  than when the quadrupole is excluded. The lines for the  $h = 0.8$  model extend down to  $\Omega_0 = 0.02$ . Results derived with both the ecliptic and galactic frame data are shown — the ecliptic frame results fall below the galactic ones at small  $\Omega_0$ . The heavy lines show the cumulative likelihood functions derived from the above likelihood densities. The quadrupole included case renders more steeply rising curves with  $h = 0.5, 0.8$  models, and galactic/ecliptic results all merge together. The less steeply rising curves, split at very small values of  $\Omega_0$ , correspond to the no quadrupole case. The 5% cumulative likelihood level is shown, as is the overall most restrictive,  $h$ - and coordinate frame-independent,  $\Omega_0 \geq 0.15$  limit on the CDM- $\Lambda$  models implied by the two year *COBE*-DMR data alone.

Fig. 3.— *a)*  $(\sigma_8)_{mass}$  values predicted from the *COBE*-DMR normalised, CDM- $\Lambda$  models, plotted as a function of  $\Omega_0 h^2$ . The  $h = 0.5, \Omega_b = 0.05$  models are shown by solid lines terminating at  $\Omega_0 h^2 = 0.25$ , while the  $h = 0.8, \Omega_b = 0.02$  lines extend to the edge

of the plot. For each model, the upper of the pair of lines corresponds to the ecliptic frame/no quadrupole analysis, whilst the lower represents the galactic frame/quadrupole included case (the remaining two combinations would lie in between). Dotted lines show the  $\Omega_b = 0.03$  results averaged over the four possible combinations. *b*) The values for the  $J_3$  integral over the density perturbation correlation function within  $20 h^{-1}\text{Mpc}$  (units  $[h^{-1}\text{Mpc}]^3$ ). Same coding as *a*. *c*) rms amplitudes of the bulk flow ( $[\text{km s}^{-1}]$ ) within spheres of 40, 60, and  $100 h^{-1}\text{Mpc}$  plotted in descending order, respectively, as a function of  $\Omega_0 h$ . Heavy lines —  $h = 0.8$ ,  $\Omega_0 = 0.02$ , thin lines —  $h = 0.5$ ,  $\Omega_0 = 0.05$ . *d*) rms amplitudes of the large scale flows ( $[\text{km s}^{-1}]$ ) as a function of the top-hat sphere radius encompassing the sample (an additional  $r_s = 1200 \text{ km s}^{-1}$  smoothing is included). Heavy lines —  $h = 0.8$ ,  $\Omega_b = 0.02$ , and  $\Omega_0 = 1, 0.4, 0.3, 0.2, 0.1, 0.05$ , and  $0.02$  in descending order. Thin lines —  $h = 0.5$ ,  $\Omega_b = 0.05$ , and  $\Omega_0 = 1, 0.4, 0.3, 0.2, 0.1$ , and  $0.05$  in descending order. The POTENT data (courtesy A. Dekel) are shown by circles, and the square denotes the Lauer & Postman datum.

Fig. 4.— *COBE*-DMR normalised inhomogeneity power spectra. The  $h = 0.5$ ,  $\Omega_b = 0.05$ , and  $h = 0.8$ ,  $\Omega_b = 0.02$  models are shown in thin and heavy lines, respectively. Dotted lines correspond to  $\Omega_0 = 1$ , CDM models. Solid lines, in descending order, show the CDM- $\Lambda$  power spectra for  $\Omega_0 = 0.1, 0.2, 0.3$  — heavy type, and  $\Omega_0 = 0.1, 0.2, 0.3$ , and  $0.4$  — light type. Overplotted are several observational estimates for the galaxy distribution power spectrum: squares - Baugh & Efstathiou (1993), filled circles - Peacock & Dodds (1994), pentagons - Fisher et al. (1993), triangles - da Costa et al. (1994) (redshift space). Miscellaneous spectral windows required for the computation of the statistics considered in this paper are shown (as annotated) as the lowermost curves. The quadrupole window depends (due to the SW and ISW effects) on model parameters,  $Q_{rms-PS}^2 = (2\pi^2)^{-1} \int dk P(k)W_Q(k)$ . For the pure Sachs-Wolfe effect,  $W_Q(k) = \Omega_0^2 H_0^4 j_2^2(kR_{LSS})/4k^2$ , where  $R_{LSS}$  is the radius of the last scattering surface (at a redshift  $z_{LSS} \simeq 1100$ ). The windows for  $\Omega_0 = 0.1, 0.3$ , and  $1$  are shown from left to right (note the trend in the window maxima and changes in the shape of the functions).

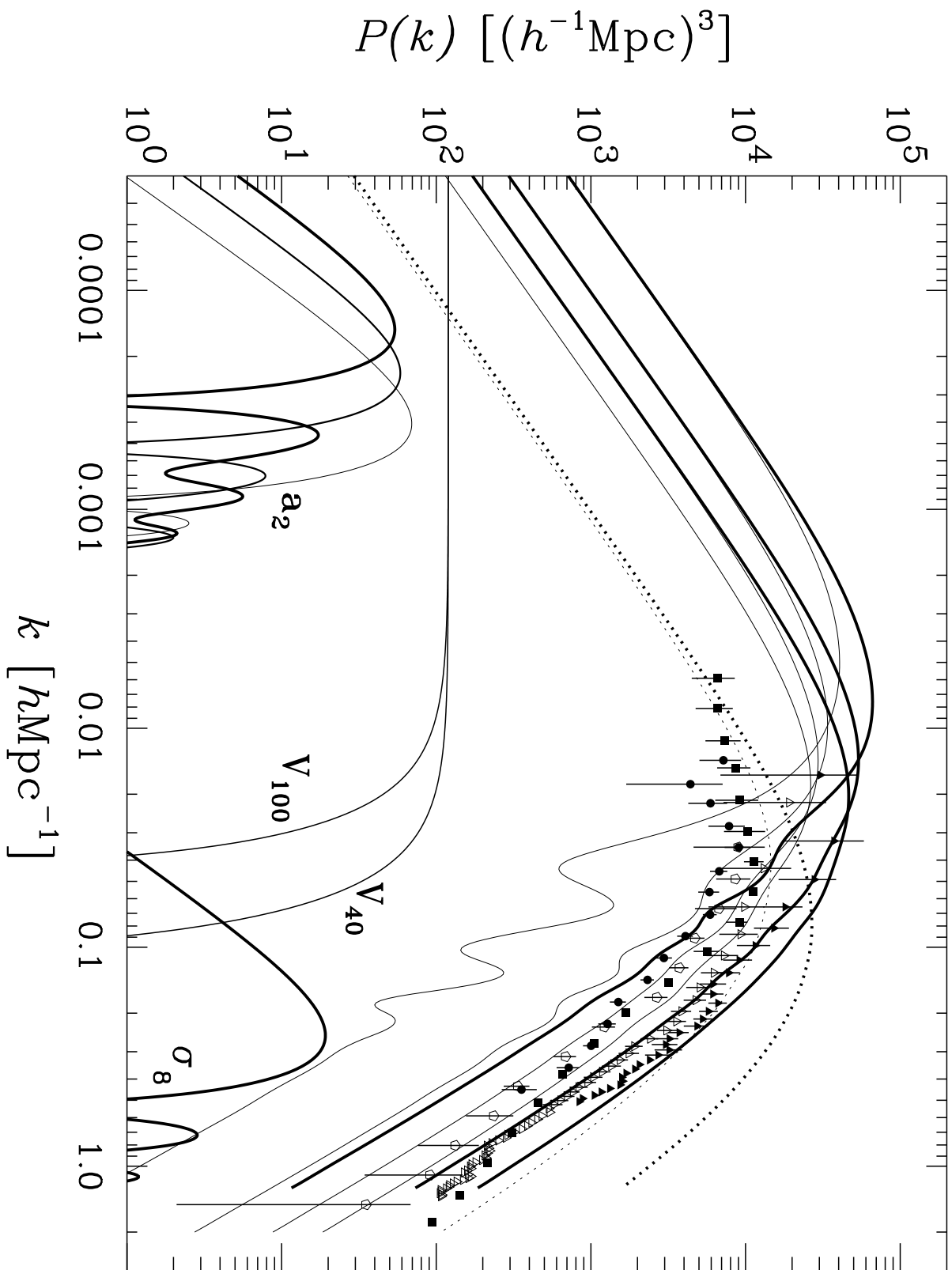


Table 1: Inferred cosmological statistics for spatially flat CDM- $\Lambda$  models with  $\Omega_b = 0.013h^{-2}$ , and a *COBE*-DMR normalisation, expressed in terms  $Q_{rms-PS}$ . The errors, including both statistical ( $1\sigma$ ) and systematic deviations, are of the order of 11%.

$\Omega_0$	$h$	$Q_{rms-PS}^{(a)}$	$\sigma_8$	$J_3^{(b)}$	$v_{40}^{(c)}$	$v_{60}^{(c)}$	$v_{100}^{(c)}$	$a_2^2/a_{2(sw)}^2^{(d)}$
0.02	0.8	28.16	0.04	4	52	51	50	2.64
0.05	0.8	27.88	0.21	66	117	113	105	2.29
	0.5	26.09	0.05	7	78	76	73	1.98
0.10	0.8	26.11	0.53	335	208	192	167	1.90
	0.5	25.27	0.17	41	139	134	123	1.64
0.20	0.8	23.61	1.03	985	330	290	230	1.46
	0.5	23.24	0.44	222	235	216	183	1.28
0.30	0.8	22.04	1.39	1496	403	342	258	1.22
	0.5	21.79	0.66	428	301	267	214	1.10
0.40	0.8	21.10	1.66	1825	449	372	272	1.09
	0.5	20.93	0.84	607	349	301	233	0.99
0.60	0.8	20.20	1.99	2081	497	398	279	0.97
	0.5	20.07	1.09	842	405	338	249	0.90
0.80	0.8	20.02	2.17	2033	513	403	276	0.94
	0.5	19.91	1.26	950	433	353	252	0.89
1.00	0.8	20.17	2.25	1859	515	399	269	0.96
	0.5	20.04	1.36	968	444	355	248	0.91

<sup>(a)</sup> in  $\mu\text{K}$ ;

<sup>(b)</sup> in  $(h^{-1}\text{Mpc})^3$ , and for  $R = 20h^{-1}\text{Mpc}$ ;

<sup>(c)</sup> in  $\text{km s}^{-1}$ .

<sup>(d)</sup>  $a_{2(sw)}$  pure Sachs-Wolfe contribution to the quadrupole.